Nanoscale Advances

ROYAL SOCIETY OF CHEMISTRY

PAPER

View Article Online
View Journal | View Issue

Cite this: *Nanoscale Adv.*, 2022, **4**, 3793

Nucleic acid-based supramolecular structures: vesicular spherical nucleic acids from a non-phospholipid nucleolipid†

Erik Dimitrov,[a] Natalia Toncheva-Moncheva,[*a] Pavel Bakardzhiev,[a] Aleksander Forys,[b] Jordan Doumanov,[c] Kirilka Mladenova,[c] Svetla Petrova,[c] Barbara Trzebicka[b] and Stanislav Rangelov[*a]

Vesicular spherical nucleic acids are dynamic nucleic acid-based supramolecular structures that are held together *via* non-covalent bonds. They have promising applications as drug and nucleic acid delivery materials, diagnostic and imaging tools and platforms for development of various therapeutic schemes. In this contribution, we report on vesicular spherical nucleic acids, constructed from a non-phospholipid nucleolipid – an original hybrid biomacromolecule, composed of a hydrophobic residue, resembling that of the naturally occurring phospholipids, and a DNA oligonucleotide strand. The nucleolipid was synthesized by coupling of dibenzocyclooctyne-functionalized oligonucleotide and azidated 1,3-dihexadecyloxy-propane-2-ol *via* an azide–alkyne *click* reaction. In aqueous solution it spontaneously self-associated into nanosized supramolecular structures, identified as unilamellar vesicles composed of a self-closed *interdigitated* bilayer. Vesicular structures were also formed upon intercalation of the nucleolipid *via* its lipid-mimetic residue in the phospholipid bilayer membrane of liposomes prepared from readily available and FDA-approved lipids (1,2-dipalmitoyl-*rac*-glycero-3-phosphocholine and cholesterol). The vesicular structures are thoroughly investigated by light scattering (dynamic, static, and electrophoretic) and cryogenic TEM and the physical characteristics, in particular, number of strands per particle, grafting density, and conformation of the strands, were compared to those of reference spherical nucleic acids. Finally, the vesicular structures were shown to exhibit cellular internalization with no need of transfection agents and enhanced colloidal and nuclease stability.

Received 8th August 2022
Accepted 8th August 2022

DOI: 10.1039/d2na00527a

rsc.li/nanoscale-advances

Introduction

Spherical nucleic acids (SNAs) are small 3D nanostructures originally composed of a gold core to the surface of which typically short (10–50 bases in length) oligonucleotide strands are covalently attached.[1,2] The latter are closely arranged and highly oriented thus forming a dense monolayer shell around the core. The spherical three-dimensional architecture of the SNAs, their sub-100 nm size, the dense arrangement and high radial orientation of the oligonucleotide strands in the shell impart specific properties that are substantially different from those of their linear counterparts. They exhibit increased colloidal stability, ability to evade immune clearance from the bloodstream, prolonged circulation time, superior cellular uptake with no need of transfection agents, higher binding affinity to complementary sequences, minimal cytotoxicity and non-specific immunogenic responses.[2–8] SNAs are a rapidly emerging class of nanoparticle-based therapeutics. They are attractive as nucleic acid delivery and gene regulation materials, intracellular diagnostics and imaging tools as well as platforms for development of various therapeutic schemes.[8–13]

SNAs have been prepared with a variety of core compositions including gold, silver, iron oxide, silica, quantum dots[2,14–22] and recent studies report on preparation of SNAs with organic cores[8,23–28] as well as hollow SNA structures. The latter represent a novel class of SNAs based on liposomal cores that are stabilized with a shell of oligonucleotide strands, intercalated *via*

[a]*Institute of Polymers, Bulgarian Academy of Sciences, Akad. G. Bonchev St. 103A, 1113 Sofia, Bulgaria. E-mail: ntoncheva@polymer.bas.bg; rangelov@polymer.bas.bg*

[b]*Centre of Polymer and Carbon Materials, Polish Academy of Sciences, M. Curie-Sklodowskiej 34, Zabrze, Poland*

[c]*Department of Biochemistry, Faculty of Biology, Sofia University St. Kliment Ohridski, Dragan Tsankov Blvd. 8, 1164 Sofia, Bulgaria*

† Electronic supplementary information (ESI) available: MALDI spectrum, HPLC chromatogram, and other characterization data of DBCO-oligonucleotide; procedures for synthesis and functionalization of 1,3-dihexadecyloxy-propane-2-ol, ^{1}H NMR and FTIR spectra; DLS data for vesicular SNAs, prepared by self-assembly of NucL2 in aqueous solution, particle size distributions by intensity, volume, and number from DLS; additional and supporting data for vesicular SNAs, prepared by co-assembly of NucL2 with DPPC and Chol, particle size distributions by intensity, volume, and number from DLS, angular dependence of relaxation rate, cryo-TEM images, particle size distribution from cryo-TEM; calculation of the Flory radius, R_F, and determination of the critical grafting density (σ_{tr}) at the transition from mushroom to brush conformation. See https://doi.org/10.1039/d2na00527a

a hydrophobic residue in the phospholipid bilayer of liposomes.[23,29] In addition to the hallmark properties of the prototypical SNAs, the liposomal SNAs have been reported to exhibit superior stability compared to the native liposomes and to inhibit the degradation of the liposomal core in the presence of serum proteins.[23] These structures are more dynamic than the prototypical SNAs, since they are held together *via* non-covalent bonds. The dynamic nature could lead to release of the hydrophobically modified oligonucleotides from the liposomal SNA structures and reach the nucleus to achieve gene regulation,[29] which constitutes an important advantage over the SNAs made from the covalent chemistry.

The development of nucleolipids, that is, hybrid molecules bearing a lipophilic moiety covalently attached to a nucleobase, nucleoside, nucleotide or oligonucleotide, is of significant interest. Not only do these molecules combine the specific chemical and biophysical properties of lipids and nucleic acids/nucleosides, but they also can develop new characteristics. Some of them derive from the amphiphilic character and self-assembling properties of the nucleolipids: they have been reported to form a variety of supramolecular structures such as monolayer films, micelles, vesicles, fibers, hydrogels, multilamellar layers,[30–36] in which the nucleobases are exposed to the aqueous phase. *Via* the lipophilic residue, they can anchor in lipidic bilayer membranes of vesicles and in the cores of micelles,[8,23,29,37–39] thereby producing novel structures, altering their properties and introducing new ones. To date most of the nucleolipids are nucleoside- or nucleotide-based, that is, they contain a single nucleic acid base. Nucleolipids, carrying an oligonucleotide strand and particularly such with a lipophilic residue featuring the phospholipid double chain are rarely described.[8,37,40,41]

In this article we report vesicular spherical nucleic acids, prepared *via* self-assembly and co-assembly of an original nucleolipid. The nucleolipid was synthesized by covalently joining a phospholipid-mimetic double chain residue with a 21-bases long nucleic acid strand using an initiator-free *click* chemistry approach. By the original design and synthetic approach we expand both the library and methods of preparation of nucleolipids. The physicochemical characterization of the nucleolipid is addressed to the study of its self-assembling and co-assembling behavior and morphological investigation of the resulting vesicular structures by means of light scattering (dynamic, static, and electrophoretic) and cryogenic electron microscopy (cryo-TEM). Preliminary biological properties (stability to enzymatic degradation, cell internalization) are presented as well.

Experimental

Materials

1-Hexadecanol (HAD, ReagentPlus®, 99%, Sigma-Aldrich), glycidyl hexadecyl ether (GHE, technical grade, Sigma-Aldrich), $SnCl_4$ (Sigma-Aldrich, 99.995% trace metals basis), potassium (cubes in mineral oil, 99.5% trace metals basis, Sigma-Aldrich), ethylene oxide (EO, ≥99.5%, Sigma-Aldrich), $MgSO_4$ (anhydrous, ReagentPlus®, ≥99.5%, Sigma-Aldrich), triethylamine (TEA, ≥99.5%, Aldrich), 4-dimethylaminopyridine (DMAP, ReagentPlus®, ≥99%, Sigma-Aldrich), methanesulfonyl chloride (MsCl, ≥99.7%, Aldrich), sodium azide (ReagentPlus®, ≥99.5%, Sigma-Aldrich), 1,2-dipalmitoyl-*rac-glycero*-3-phosphocholine (DPPC, ~99%, Sigma-Aldrich), cholesterol (Chol, Sigma Grade, ≥99% Sigma-Aldrich), 1,6-diphenyl-1,3,5-hexatriene (DPH, 98%, Sigma-Aldrich) were used as received. Hexane (anhydrous, 95% Sigma-Aldrich), methylene chloride (>99.98%, Fisher Scientific), toluene (>99.8%, Fisher Scientific), and tetrahydrofuran (THF, >99.5%, Fisher Scientific) were dried with calcium hydride and freshly distilled before use. *N*,*N*-Dimethylformamide, (DMF, ACS reagent, ≥99.8%) and dimethyl sulfoxide (DMSO, ACS reagent, ≥99.9%) were dried by molecular sieves. A dibenzocyclooctyne-functionalized oligonucleotide (DBCO-oligonucleotide) was purchased from (**https://Biomers.net**) GmbH. The sequences and composition of DBCO-oligonucleotide as well as a MALDI spectrum and a HPLC chromatogram are presented in the ESI (Table SI1 and Fig. SI1).† Deionized water was obtained by a Millipore Milli-Q system and was additionally filtered through a 220 nm PTFE filter and a 20 nm cellulose filter. Chemicals for biological evaluation are analytical grade purchased from Merck (Kenilworth, USA): Dulbecco's modification of Eagle's medium/nutrient mixture F-12 Ham (DMEM F-12 Ham), Fetal Calf Serum (FCS), 2-(4,5-dimethyl-2-thiazolyl)-3,5-diphenyl-2*H*-tetrazolium bromide (MTT), Penicillin, Streptomycin, Crystal violet dye and DNases.

Synthetic procedures

Synthesis of 1,3-dihexadecyloxy-propane-2-ol (DHP). DHP was synthesized following a procedure described elsewhere.[42,43] Details for the synthetic procedure are given in ESI.†

Synthesis of DHP-$(EO)_6$-CH_2CH_2OH. 1 g of DHP (1.852 mmol, 1 eq.) were dissolved in 10 mL of anhydrous THF in a 50 mL flask. The flask was flushed with nitrogen and 72 mg (1.852, 1 eq.) of potassium metal were added to the solution. The mixture was left for 24 hours at 40 °C during which all the alkali metal was dissolved. The content of the flask was taken out through the rubber septum *via* syringe and placed in a thick-walled ampoule. After cooling to −70 °C, 650 μL (14.8 mmol, 8 eq.) of liquid ethylene oxide were added *via* a cooled Hamilton microsyringe and the ampoule was sealed while still cold and left for 24 hours at room temperature. Upon completion of the reaction, the ampoule was opened and the content was poured in 70 mL of water. The mixture was extracted three times with 40 mL of methylene chloride and the combined extracts were dried with anhydrous $MgSO_4$. Evaporation of the solvent gave 1.25 g of DHP-$(EO)_6$-CH_2CH_2OH, 76% yield.

Synthesis of DHP-$(EO)_6$-CH_2CH_2OMs. 1.2 g of DHP-$(EO)_6$-CH_2CH_2OH (1.41 mmol, 1 eq.), 1.42 g of TEA (14.1 mmol, 10 eq.) and 0.086 g of DMAP (0.71 mmol, 0.5 eq.) were dissolved in 20 mL of anhydrous methylene chloride in a 50 mL round-bottom flask. The solution was cooled to 0 °C and flushed with nitrogen, after which 1.62 g of MsCl (14.1 mmol, 10 eq.) in 10 mL of methylene chloride were added. The reaction mixture was left for 24 hours at room temperature and then poured to 100 mL of water. The organic layer was separated and the

remaining was extracted 3 times with a small amount of methylene chloride. The combined extracts were dried with anhydrous $MgSO_4$. Evaporation of the solvent gave 0.875 g of DHP-$(EO)_6$-CH_2CH_2OMs, 67% yield.

Synthesis of DHP-$(EO)_6$-$CH_2CH_2N_3$. 0.8 g of DHP-$(EO)_6$-CH_2CH_2OMs (0.862 mmol, 1 eq.) were dissolved in 15 mL of a DMSO/DMF (v/v 2/1) mixture and 0.84 g (12.93 mmol, 15 eq.) of NaN_3 were added to the solution. The mixture was heated to 50 °C for 20 hours and after that poured in 70 mL of water. The solution was extracted 3 times with 50 mL of hexane. The combined extracts were dried with anhydrous $MgSO_4$, concentrated to about 50 mL and cooled to −35 °C to precipitate the product. Cold filtration and drying gave 0.670 mg of pure DHP-$(EO)_6$-$CH_2CH_2N_3$, 90% yield.

Synthesis of DHP-$(EO)_6$-oligonucleotide conjugate (NucL2). DBCO-oligonucleotide (724.4 μg, 101.04 nmol, 1 eq.) was dissolved in a 1.25 mL mixture of DMF/DMSO (v/v 1/1) and placed in a round-bottom flask under argon atmosphere. The solution was purged with argon and stirred vigorously for 20 min. Separately, pure DHP-$(EO)_6$-$CH_2CH_2N_3$ (220 μg, 252 nmol, 2.5 eq.) was dried by azeotropic distillation in toluene. The dry product was dissolved in 1.25 mL of a dry organic solvent mixture (DMSO/DMF, v/v 1/1) and added *via* a syringe to DBCO-oligonucleotide solution. The azide–alkyne click coupling reaction was carried out under argon at 40 °C for 36 h. The reaction mixture was cooled to room temperature and purified by intense dialysis against the DMSO/DMF mixture for 2 days using dialysis tubes with a molecular weight cut-off (MWCO) of 7 kDa membrane.

Preparation of vesicular SNAs by self-assembly of NucL2. NucL2 vesicles were obtained by the solvent displacement method. The solution of NucL2 in DMSO/DMF was dialyzed against ultra-pure Milli-Q water for 3 days and then purified by ultrafiltration, which yielded a colorless slightly opalescent aqueous dispersion of NucL2 nanoparticles.

Preparation of vesicular SNAs by co-assembly of DPPC, Chol, and NucL2. Stock solutions of known concentrations of DPPC and Chol in chloroform and NucL2 in methanol were prepared. Predefined amounts of these solutions were placed into glass tubes to achieve 2 mM total lipid concentration, 2 : 1 DPPC : Chol molar ratio, 2 mol% of NucL2 as follows: 0.04 μmol (304.88 μg) of NucL2, 1.30 μmol (954.2 μg) of DPPC, and 0.65 μmol (251.55 μg) of Chol. The solvent ratio was kept in the 1 : 9–1 : 10 range with respect to methanol in order to avoid precipitation. The solvent was removed under a gentle stream of argon leaving a thin film. All traces of solvent were removed under vacuum overnight at room temperature. The dry thin lipid film was hydrated with 1 mL of Mili-Q water and the resulting dispersion was subjected to ten freeze–thaw cycles and then extruded 15 times through polycarbonate filters (100 nm pore size) using a handle type extruder (Avanti Polar Lipids, USA).

Methods

Nuclear magnetic resonance (^{1}H-NMR). ^{1}H-NMR measurements were conducted on a Bruker Avance II spectrometer operating at 600 MHz using $CDCl_3$ or DMSO-d_6 at 25 °C.

Light scattering. Dynamic light scattering (DLS) measurements were performed on a Brookhaven BI-200 goniometer with vertically polarized incident light at a wavelength $\lambda = 633$ nm supplied by a He–Ne laser operating at 35 mW and equipped with a Brookhaven BI-9000 AT digital autocorrelator. The scattered light was measured for dilute aqueous dispersions of NucL2 in the concentration range 0.0398–0.0636 mg mL^{-1} at 25 °C. Measurements were made at angles θ in the range of 50–130°. The autocorrelation functions were analyzed using the constrained regularized algorithm CONTIN[44] to obtain the distributions of the relaxation rates (Γ). The latter provided distributions of the apparent diffusion coefficient ($D = \Gamma/q^2$) where q is the magnitude of the scattering vector given by $q = (4\pi n/\lambda)\sin(\theta/2)$, n is the refractive index of the medium. The mean hydrodynamic radius was obtained by the Stokes–Einstein eqn (1):

$$R_h = kT/(6\pi\eta D_0) \quad (1)$$

where k is the Boltzmann constant, η is the solvent viscosity at temperature T in kelvin and D_0 is the diffusion coefficient at infinite dilution.

Static light scattering (SLS) measurements were carried out in the interval of angles from 40 to 140° at 25 °C using the same light scattering set. The SLS data were analyzed using the Berry plot software provided by Brookhaven Instruments. Information on the weight-average molar mass, M_w, the radius of gyration, R_g, and the second virial coefficient, A_2, was obtained from the dependence of the quantity $(K_c/R_\theta)^{1/2}$ on the concentration (c) and scattering angle (θ). Here, K is the optical constant given by $K = 4\pi^2 n_0^2 (dn/dc)^2/N_A\lambda^4$, where n_0 is the refractive index of the solvent, N_A is Avogadro's constant, λ is the laser wavelength, and R_θ is the Rayleigh ratio at θ. dn/dc is the refractive index increment measured in water in separate experiments on an Orange GPC19 DNDC refractometer. The dn/dc value of the investigated system was 0.142 mL g^{-1}.

Static and dynamic light scattering parameters of DPPC/Chol/NucL2 SNAs were determined at a single concentration.

Electrophoretic light scattering. The electrophoretic light scattering measurements were carried out on a 90Plus PALS instrument (Brookhaven Instruments Corporation), equipped with a 35 mW red diode laser ($\lambda = 640$ nm) at a scattering angle (θ) of 15°. ζ potentials were calculated from the obtained electrophoretic mobility at 25 °C by using the Smoluchowski equation (2):

$$\zeta = 4\pi\eta\upsilon/\varepsilon \quad (2)$$

where η is the solvent viscosity, υ is the electrophoretic mobility, and ε is the dielectric constant of the solvent.

Cryogenic transmission electron microscopy (cryo-TEM). cryo-TEM images were obtained using a Tecnai F20X TWIN microscope (FEI Company, Hillsboro, Oregon) equipped with a field-emission gun, operating at an acceleration voltage of 200 kV. Images were recorded on the Gatan Rio 16 CMOS 4k camera an Eagle 4k HS camera (Gatan Inc., Pleasanton, California, USA) and processed with Gatan Microscopy Suite (GMS) software

(Gatan Inc., Pleasanton, California, USA). Specimen preparation was done by vitrification of the aqueous dispersions on grids with a holey carbon film (Quantifoil *R* 2/2; Quantifoil Micro Tools GmbH, Groβlöbichau, Germany). Prior to use, the grids were activated for 15 s in oxygen plasma using a Femto plasma cleaner (Diener Electronic, Ebhausen, Germany). cryo-Samples were prepared by applying a droplet (3 μL) of the dispersion to the grid, blotting with filter paper and immediate freezing in liquid ethane using a fully automated blotting device Vitrobot Mark IV (Thermo Fisher Scientific, Waltham, Massachusetts, USA). After preparation, the vitrified specimens were kept under liquid nitrogen until they were inserted into a cryo-TEM holder Gatan 626 (Gatan Inc., Pleasanton) and analyzed at −178 °C.

Gel electrophoresis. The completeness of the click coupling reactions and formation of aggregates were confirmed by agarose gel electrophoresis. Gels containing 1% agarose (w/w) were run on an FBSB-710 electrophoresis unit (Fisher Biotech) in 1× Tris-Borate EDTA (TBE) buffer at room temperature and 50 V. Imaging was carried out by ethidium bromide staining and UV illumination (302 nm). The gels were imaged using a gel reader Alpha Innotech. Quick-Load® Purple 1 kb DNA Ladder of BioLabs was used as a marker.

Cell cultures. A549 (human lung carcinoma) cells were grown in DMEM with 10% (v/v) FCS, streptomycin (0.1 mg mL^{-1}), penicillin (0.06 mg mL^{-1}) at 37 °C in 5% CO_2 water-saturated atmosphere.

Immunofluorescent staining. 1×10^5 A549 cells per well were seeded in 24 well plates for 24 h at 37 °C before treatment with vesicular DPPC/Chol/NucL2 SNAs containing 0.2 mol% with respect to the total lipid content of DPH ($\lambda_{ex} = 353$ nm; $\lambda_{em} = 430$ nm). The cells were incubated with vesicular DPPC/Chol/NucL2 SNAs at a concentration of 0.2 μg of oligonucleotides per well for 30 min and immediately after treatment the nanoparticles in alive cells were visualized by fluorescent Microscope (GE Delta Vision Ultra Microscopy System).

DNase activity assay. Endonuclease activity of DNase I (EC 3.1.21.1) on the two vesicular SNAs was assayed using the manufacturers' instructions and compared with DNase I activity on free oligonucleotides as described elsewhere.[45,46] One enzyme unit was defined as the amount of DNase I added to 1 mg mL^{-1} of oligonucleotides, that causes an increase of 0.001 absorbance units at 260 nm per min when assayed in a 0.1 M NaOAc (pH 5.0) buffer, containing 4.2 mM magnesium sulfate and 25 mM sodium chloride.

Results and discussion

Nucleolipid synthesis and characterization

To develop vesicular structures, stabilized by a shell of oligonucleotides, we designed a novel nucleolipid (hereinafter, NucL2), composed of a hydrophobic lipid-mimetic double chain moiety and a hydrophilic DNA oligonucleotide strand. The novel nucleolipid is amphiphilic: it is expected to self-associate into nanosized aggregates and to intercalate *via* its lipid-mimetic residue (anchor) between the phospholipids. The synthesis of NucL2 was realized by an azide–alkyne *click* reaction, which is a straightforward and high yielding approach.

In a typical synthesis, the lipid-mimetic anchor, 1,3-dihexadecyloxy-propane-2-ol (DHP), prepared as described elsewhere[42,43] (see also ESI, Fig. SI2 and SI3),† was modified by ethoxylation of the hydroxyl group, thus introducing a short spacer of an average of 6 EO units – DHP-$(EO)_6$-CH_2CH_2OH (Scheme 1a). This intermediate was obtained by anionic polymerization of EO and the average number of EO units of the spacer was determined from the ^{1}H NMR spectrum of the purified product (Fig. 1). DHP-$(EO)_6$-CH_2CH_2OH was mesylated (Scheme 1b) by a reaction with methanesulfonyl chloride and, in the final step, the mesylate group was converted into azide to obtain DHP-$(EO)_6$-$CH_2CH_2N_3$ (Scheme 1b). The successful transformations of the end hydroxyl group into mesylate and azide groups were proved by ^{1}H NMR (Fig. 1). Together with all characteristic signals assigned for the structure of DHP-$(EO)_6$-CH_2CH_2OH (Fig. 1a), a new signal at 3.09 ppm corresponding to methylene protons adjacent to the mesylate end group appeared (Fig. 1b). Upon azidation, a new signal at 3.39 ppm, assigned to the methylene protons adjacent to the azide end group, was detected, while the signal at 3.09 ppm completely disappeared (Fig. 1c). In addition, the integral ratio of the proton signals from CH_2N_3 (2H at 3.39 ppm) and the end methyl end groups of DHP (6H at 0.88 ppm) was almost equal to the theoretical value 2 : 6.

The introduction of a spacer was of key importance because the transformation of the secondary hydroxyl group of DHP into mesylate and azide groups has proven unsuccessful (see ESI, Fig. SI4–SI6).† To obtain the nucleolipid, a proper excess of the intermediate DHP-$(EO)_6$-$CH_2CH_2N_3$ and dibenzocyclooctyne-terminated DNA oligonucleotide strands, both in a solvent mixture DMSO/DMF (v/v 1/1), were added to initiate the copper-free azide–alkyne click reaction (Scheme 1c). The resulting conjugate (nucleolipid NucL2) was purified by dialysis and ultrafiltration by which the excess of the azidated compound was removed.

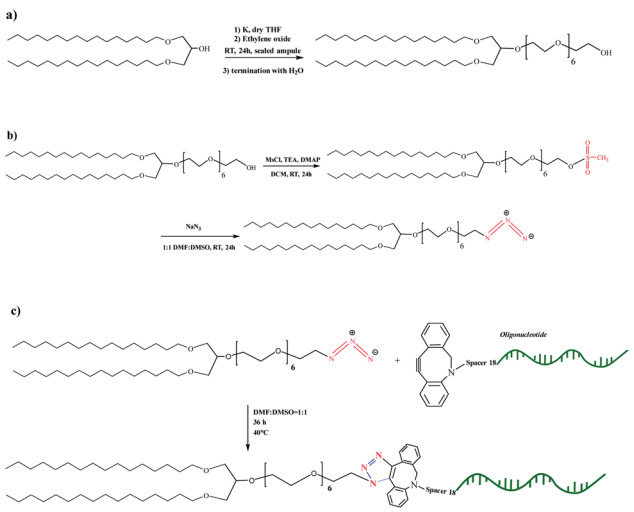

Scheme 1 Synthetic scheme for the preparation of the intermediates DHP-$(EO)_6$-CH_2CH_2OH (a), DHP-$(EO)_6$-$CH_2CH_2OSO_2CH_3$ and DHP-$(EO)_6$-$CH_2CH_2N_3$ (b), and the nucleolipid NucL2 (c).

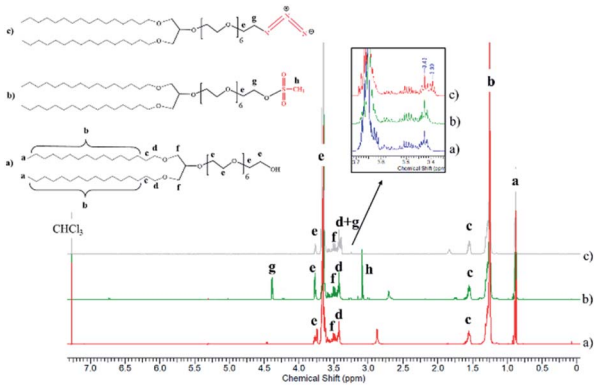

Fig. 1 ^{1}HNMR spectra of the intermediates DHP-$(EO)_6$-CH_2CH_2OH (a), DHP-$(EO)_6$-$CH_2CH_2OSO_2CH_3$ (b) and DHP-$(EO)_6$-$CH_2CH_2N_3$ (c) in $CDCl_3$ (600 MHz).

Agarose gel electrophoresis was used to analyze the resulting nucleolipid (Fig. 2). Before that, the mixed DMSO/DMF solvent was displaced by dialysis against ultrapure water, which yielded a slightly opalescent aqueous dispersion of NucL2. As evident from Fig. 2, the electrophoretic mobility of NucL2 was retarded compared to that of DBCO-oligonucleotide, used as control, which was consistent with the enlargement of the molecular weight of NucL2. Notably, a second band was clearly observed, indicating formation of another population of particles with mobility that was further reduced compared to that of the major band.

Aqueous solution properties

Formation of vesicular SNAs by self-assembly of nucleolipid molecules. The additional band in the gel images (Fig. 2) clearly indicated formation of a second fraction – presumably multimolecular aggregates significantly larger in size and/or overall charge compared to those responsible for the major band. Multiangle dynamic and static light scattering experiments were carried out to characterize the particles that NucL2 formed. In the range of concentrations that are slightly higher than the concentration for the agarose gel electrophoresis, a monomodal relaxation time distribution from DLS was invariably observed (Fig. 3a) corresponding to existence of only one population of particles with apparent diameters of about 220–230 nm. Particle size distributions, converted from relaxation time distributions, are shown in the ESI (Fig. SI7).† The *z*-average diffusion coefficients were obtained from the angular dependences of the relaxation rate (inversely proportional to relaxation time), measured at different scattering angles (Fig. 3b). The diffusion coefficients were plotted against concentration and extrapolated to zero concentration to obtain the value of the diffusion coefficient at infinite dilution, D_0 (Fig. 3c), which was used to calculate the hydrodynamic radius, R_h, applying the Stokes–Einstein equation (eqn (1)). Assuming spherical morphology of the NucL2 aggregates, eqn (1) gave a value of R_h of 115.1 nm (Table 1).

SLS was performed in the same concentration range as DLS. The static parameters – weight-average molar mass (M_w), radius of gyration (R_g), and second virial coefficient (A_2) – were evaluated by the Berry plot method. The Berry diagram for NucL2 is presented in Fig. 3d, whereas the derived static light scattering parameters are collected in Table 1. Evident from the results in Table 1 is that NucL2 in aqueous solution formed relatively large particles (radii of above 110 nm) with a weight-average molar mass reaching 709 × 10^6 g mol^{-1}, corresponding to aggregation number, N_{agg}, of about 88 000 molecules per particle. In accordance with the high M_w, A_2 is very small (of the order of 10^{-7}) but positive, indicating favorable particle–solvent interactions. The particles exhibited strongly negative ζ potential (−31.9 mV, Table 1), which was consistent with the anionic

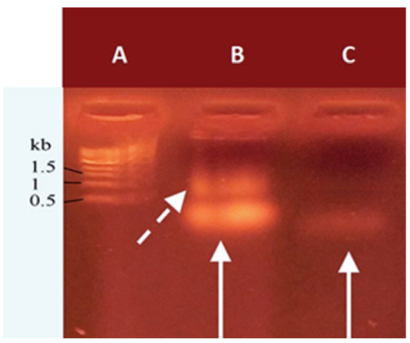

Fig. 2 Agarose gel retardation analysis of DBCO-functionalized oligonucleotide (lane C) and NucL2 (lane B). The solid arrows indicate the different retardations of the functionalized oligonucleotide and nucleolipid. The dashed arrow indicates appearance of a fraction of supramolecular particles. Nucleic acids were stained with ethidium bromide. Overall duration of the experiment: 20 min. Lane A: molecular weight marker. Total amounts of 6 μg and 0.6 μg were loaded in B and C, respectively.

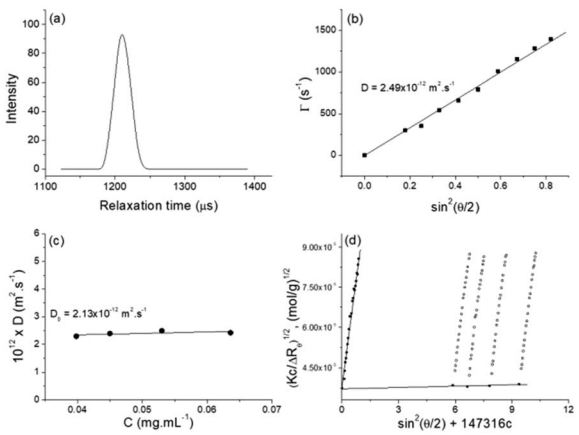

Fig. 3 (a) Representative relaxation time distribution (τ), measured at an angle of 90° for aqueous solution of NucL2 at concentration of 0.0398 mg mL^{-1}. (b) Relaxation rate (Γ) as a function of $\sin^2(\theta/2)$ for NucL2 at concentration of 0.053 mg mL^{-1}. (c) Concentration dependence of diffusion coefficients for NucL2. The lines through the data points in (b) and (c) represent the linear fit to the data. (d) Berry plot of NucL2 in aqueous solution. Open symbols and closed symbols represent experimental points and extrapolated points to zero concentration and zero angle, respectively. Measurements were performed at 25 °C.

Table 1 Static, dynamic, and electrophoretic light scattering characterization data of vesicular SNAs, prepared from the nucleolipid NucL2

Parameters	R_h (nm)	R_g (nm)	R_g/R_h	$10^7 \times A_2$ (mL mol g^{-2})	$10^{-6} \times M_w$ g mol^{-1}	$10^{-4} \times N_{agg}$	ζ (mV)
Value	115.1 ± 3.4	112.0 ± 2.8	0.97	7.20 ± 0.39	709.0 ± 33.0	8.8 ± 0.4	−31.9

nature of the hydrophilic portion of the nucleolipid – the oligonucleotide strands.

An obvious question that arose from the results was what the structure of the particles that NucL2 formed is. The nucleolipids are known to form a variety of supramolecular structures, including particulate structures such as micelles, vesicles, and fibers.[30–36] The NucL2 aggregates cannot be core–corona micelles because of their large size: the radius of the particles is much larger than the length of the fully stretched molecule of NucL2. Furthermore, huge molar masses and aggregation numbers have been observed for vesicles, liposomes, and bilayer structures.[43,47,48] In addition R_g/R_h attained a value close to unity (Table 1), which was consistent with vesicular structures.[49,50] In order to resolve the morphology of the particles formed by NucL2, we performed cryo-TEM. Fig. 4 shows single objects with clearly distinguishable rims at the outermost periphery, evidencing the vesicular structure of the particles. They are of spherical (though not perfect) morphology with dimensions in a reasonable agreement with those obtained by DLS. The vesicles are single-walled with no internal structure. The bilayer membrane looked intact, that is, openings and perforations were not observed.

After having established that the aggregates were vesicles, from DLS and SLS results, we may calculate the mean area occupied by NucL2 molecule in the bilayer. From the total area of the vesicular bilayer and aggregation number, a value of 3.8 nm^2 per molecule was obtained, which might look higher than what is realistic even for nucleolipids with a relatively long oligonucleotide strand. To rationalize the results, we may speculate on interdigitation of the bilayer. A schematic representation of an interdigitated bilayer is given in Scheme 2. A prerequisite for formation of this phase is strong repulsion between the lipid heads, which seemed to be present in the system: the oligonucleotide strands (as lipid heads) are negatively charged and may experience repulsive electrostatic interactions. Furthermore, 100% of the lipid heads are oligonucleotide strands (no other lipid molecules in the bilayer). Hristova and Needham in an earlier paper predicted that interdigitation was likely to occur for PEG (poly(ethylene glycol) as a hydrophilic head of PEG-lipids) of molar mass of 350 at contents of about 30 mol% and at lower molar percent for higher molar mass PEG.[51] With molar mass of oligonucleotide strands of more than 7000 (see Table SI1†) and 100% grafting, it is very likely that the oligonucleotide strands are in the brush regime. Thus, interdigitation of the bilayer would increase the area per NucL2 molecule and would relax the lateral pressure between the strands.

Formation of vesicular SNAs by co-assembly of the nucleolipid NucL2 and lipids. Novel, hybrid structures were prepared by co-assembly of NucL2 with the lipids 1,2-dipalmitoyl-*sn*-*glycero*-phosphocholine (DPPC) and cholesterol (Chol). The total lipid concentration was 2 mM at a 2 : 1 DPPC : Chol molar ratio, whereas the NucL2 content was fixed to 2 mol%. The dispersions were prepared by hydration of a dry thin film. Afterwards, they were subjected to 10 freeze–thaw cycles and extruded through polycarbonate filters of pore size 100 nm. The dispersions appeared slightly/moderately opalescent and remained optically clear for weeks. Defining factors to avoid individual self-assembly of the components and/or their separation within the bilayer membrane were the Chol content along with the method of preparation of the structures. It has been shown that at concentration of 33.3 mol% Chol is completely miscible with DPPC and induce formation of a liquid-ordered phase.[52–54] Furthermore, the preparation procedure ensures effective mixing of all constituents thereby maximizing the equal distributions of various polymer-derivatized lipids in the outer and inner leaflets of the bilayer and homogeneity of the liquid-ordered phase.[55–58]

DLS study showed monomodal size distributions with very narrow polydispersity indices typically below 0.1. A representative size distribution is presented in Fig. 5a. More particle size distributions are shown in Fig. SI8.† The diffusion coefficient was determined from the angular dependence of the relaxation rate as shown above (see also Fig. SI9 in the ESI†) and then

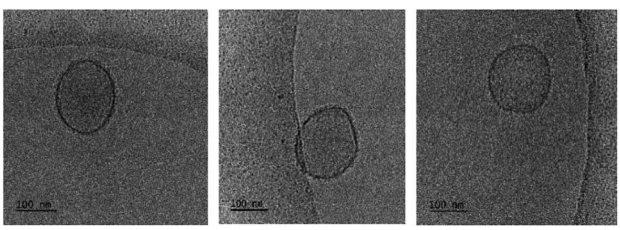

Fig. 4 cryo-TEM micrographs of vesicles taken from aqueous dispersions of NucL2.

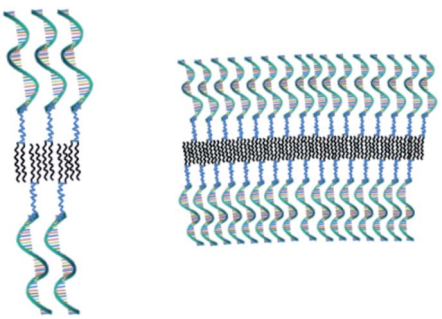

Scheme 2 Schematic representation of small (left) and large (right) sections of an interdigitated bilayer of vesicular SNAs, prepared from the nucleolipid NucL2.

converted into apparent hydrodynamic radius. The radius of gyration was determined from the partial Berry plot (Fig. 5b). The two parameters, along with the R_g/R_h ratio and ζ potential, are presented in Table 2.

The particles were visualized by cryo-TEM (Fig. 5c). More images as well as particle size distributions are presented in the ESI (Fig. SI10).† The dominating structures are clearly unilamellar vesicles of spherical morphology. Bilamellar vesicles and vesicles of irregular (non-spherical, *e.g.*, ellipsoidal) morphology were only occasionally observed. The average size (average diameter of about 140 nm), measured from cryo-TEM, was in very good agreement with that obtained from DLS (*cf.* Fig. 5a, SI11, and Table 2 in ESI†). The bilayer membrane looked intact, *i.e.*, openings or any kind of damages were not detected. It is of constant thickness of about 5 nm (see the ESI†), which is compatible with DPPC systems.[59,60] The background of the images was clear and small material, *e.g.*, bilayer fragments or other, non-bilayer structures, was not observed.

The method for preparation of the dispersions, in particular, the step of multiple extrusion through filters of pore size 100 nm, is known to yield unilamellar liposomes with a mean hydrodynamic radius of about 50–60 nm.[55,56] In that aspect, the incorporation of NucL2 in the bilayer membrane was marginal, since it resulted only in a slight increase of R_h (Table 2). However, the other two parameters – the quantity R_g/R_h and ζ potential – were more strongly affected. The former increased from a unity, which is typically obtained for large unilamellar vesicles,[49,50] to a value of 1.17, whereas the latter shifted to a more negative value (Table 2), compared to DPPC/Chol liposomes.[61,62] The changes in these parameters can apparently be associated with successful incorporation of the nucleolipid in the bilayer membrane and formation of an outer shell of oligonucleotide strands. The bilayer membrane, however, must be grafted on both sides as the vesicles were obtained by simultaneous association of the lipids and NucL2 *via* rehydration of a mixed DPPC/Chol/NucL2 thin film. In other words, there must be a portion of oligonucleotide strands in the interior of the vesicles forming an inner shell. A schematic illustration of a vesicle is presented in Scheme 3.

Since the unique properties of the prototypical SNAs stem from the density and orientation of the oligonucleotides in the outer region of the nanostructures, questions arise what is the grafting density of the oligonucleotide strands in the present vesicular SNAs, how dense is the shell, and what is the conformation/orientation of the strands in the shell. The grafting density, σ, was determined from the number of oligonucleotide strands and total bilayer area. The total bilayer area was calculated from the hydrodynamic radius from DLS. Then, assuming an average area of 0.65 nm^2 per both DPPC and nucleolipid, which is a reasonable value,[60] we calculated the aggregation number, N_{agg}, from which the number of nucleolipid molecules (hence, oligonucleotide strands) was determined knowing the nucleolipid content in the formulation (2 mol%) upon the assumption that the nucleolipid is equally distributed in all vesicles. The results are collected in Table 2. As seen, the average number of oligonucleotide strands per vesicle is about 3430, which is relatively higher than that of reference SNAs, including micellar and liposomal SNAs as well as gold nanoparticle SNAs[26,63–65] and can be attributed to the larger size of the present vesicular SNAs. This value was converted into grafting density, expressed as a number of strands per nm^2. The resulting value of $\sigma = 0.031\ nm^{-2}$ was slightly lower than those of reference samples,[26,63–65] implying somewhat lower density of the shell. It is noteworthy that both the number of oligonucleotide strands per vesicle and the grafting density refer to this particular formulation (DPPC/Chol/Nucl2 65.3/32.7/2.0 mol ratio) and would increase upon increasing nucleolipid content.

An interesting although somewhat expected finding was that the grafting density was apparently lower than the critical grafting density, σ_{tr}, implying that the oligonucleotide strands are isolated and non-interacting each other in the shell. σ_{tr} is the grafting density at which surface-anchored polymer coils (or the oligonucleotide strands in the present system) start to interact laterally and a transition from mushroom to brush conformation takes place. σ_{tr} ($= 0.117\ nm^{-2}$) for the nucleolipid was estimated from the Flory radius of the oligonucleotide strand as shown in the ESI.† It must be noted here that the critical values of σ_{tr} have never been reached even for reference SNAs as discussed elsewhere.[66] Nevertheless, these structures have been shown to manifest the unique properties of SNAs.

Nuclease stability and cell internalization. The biological relevance of the vesicular SNAs was evaluated in terms of resistance to enzymatic degradation and cell internalization, which are typical, hallmark properties of the SNAs. As noted in the previous sections the two vesicular SNAs exhibit remarkable colloidal stability. The shelf stability (4 °C and sterile conditions) was within at least two months during which changes in the characterization parameters were practically not detected. The enhanced stability can be attributed to the formation of a shell of oligonucleotide strands that experience electrostatic repulsive interactions. This shell, which is common to all types of SNAs (*e.g.*, gold nanoparticle SNAs, micellar and liposomal SNAs), has been hypothesized to enhance the resistance to nuclease degradation due to steric hindrance, which limits the

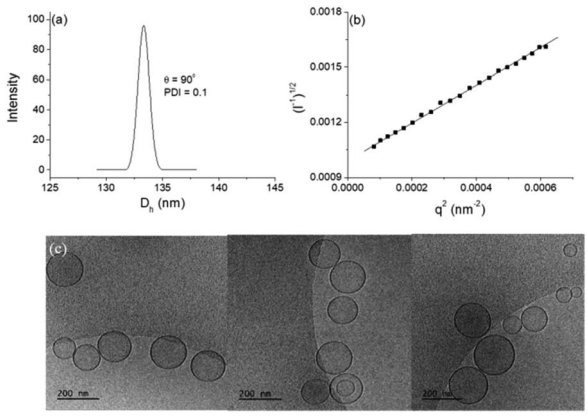

Fig. 5 Particle size distribution from DLS, measured at an angle $\theta = 90°$ (a) and partial Berry plot (b) of DPPC/Chol/NucL2 vesicles at $c = 2$ mM total lipid. Measurements were performed at 25 °C. (c) cryo-TEM images of DPPC/Chol/NucL2.

Table 2 LS parameters and other data for vesicular SNAs prepared by co-assembly of DPPC, cholesterol and NucL2 at molar ratio 65.3/32.7/2.0

Parameter	R_h[a] (nm)	R_g[b] (nm)	R_g/R_h	ζ (mV)	Total bilayer area (nm^2)	N_{agg}[c]	Number of oligo-nucleotides per vesicle	σ[d] (nm^{-2})
Value	66.6 ± 0.9	78.0 ± 0.3	1.17	−17.8 ± 0.5	111 480 ± 3000	171 500 ± 4600	3430 ± 92	0.031

[a] Determined from the angular dependence of the relaxation rate at a single concentration. [b] Determined from the partial Berry plot at a single concentration. [c] Aggregation number. [d] Grafting density.

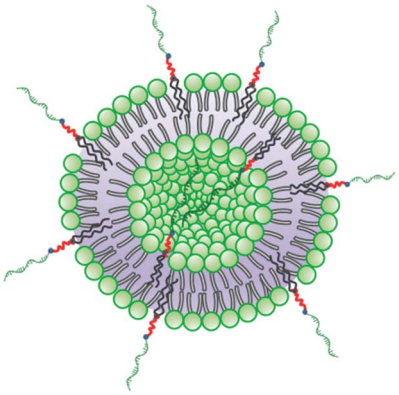

Scheme 3 Schematic illustration of a vesicular SNA formed by co-assembly of DPPC, Chol, and NucL2.

exposure of the oligonucleotide strands to the enzyme.[3,67,68] The stability of NucL2 and DPPC/Chol/NucL2 vesicles was tested against the endonuclease DNase I.[69] The results are presented in Fig. 6. It is noteworthy that the nucleolipid NucL2 was tested at concentration within the concentration range of the agarose gel electrophoresis experiments (*i.e.*, below the concentration range at which vesicular structures were detected and characterized, see section Aqueous solution properties). At lower concentrations and upon dilution, one may anticipate decomposition of the self-assembled structures and formation of two co-existing phases – unimers (unassociated NucL2 molecules) and vesicles. The results show that the DNase enzyme specific activity towards NucL2 as a substrate was lower by about 30% compared to the control unmodified oligonucleotides of the same number of bases. Obviously, the arrangement of DNA oligonucleotides on the surface of the structures reduces the access of DNase I to the oligonucleotides, which results in lowering of enzyme specific activity and, hence, enhancement of the nuclease stability of the vesicular structures. A further reduction of the nuclease activity might be expected upon increasing NucL2 content in the DPPC/Chol/NucL2 vesicles, which would result in an increase of the grafting density, or upon increasing NucL2 concentration leading to a shift of the equilibrium unimers-vesicles to the vesicular phase.

The rapid cellular uptake without the need of transfection agents is another, probably the most important, property of the SNAs.[2] To examine this property, A549 cells were incubated with DPPC/Chol/NucL2 vesicles. The vesicles were firstly treated with 1,6-diphenyl-1,3,5-hexatriene (DPH) – a fluorescent compound widely utilized in studies of membrane interiors and fluidity.[70,71] It is practically non-fluorescent in water, but when intercalated into membranes, exhibits a strong increase in fluorescence. Thus, by labeling the bilayer membranes of the DPPC/Chol/NucL2 vesicles it was possible to follow the *in vitro* cell uptake. Remarkably, the vesicles entered A549 cells readily even after a very short (30 min) incubation time (Fig. 7). After internalization, the negatively charged DPPC/Chol/NucL2 vesicles were observed as small granules (blue dots), denoted by arrows

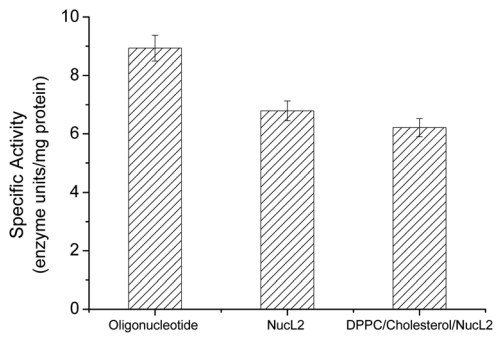

Fig. 6 DNase enzyme specific activity against oligonucleotide, nucleolipid NucL2, and DPPC/cholesterol/NucL2 (65.3/32.7/2.0 mol ratio) vesicles.

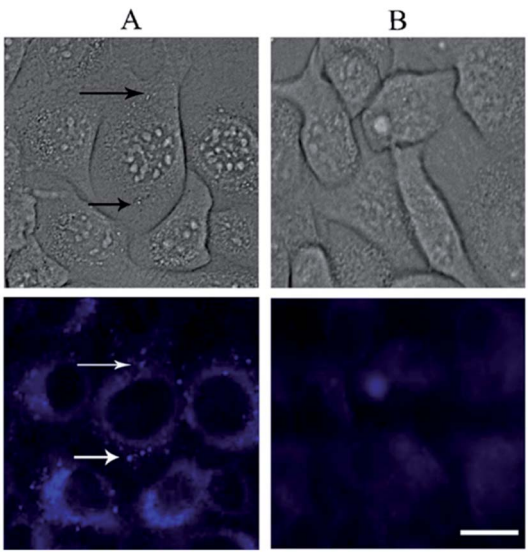

Fig. 7 White light (up) and fluorescent (low) micrographs of A549 cells following 30 min exposure to DPPC/Chol/NucL2 vesicles (panel A). The vesicles taken up by the cells are indicated by arrows. Imaging results with A549 cells that have not been treated with the vesicles (control) are shown in panel B. Scale bar 15 μm applies for all images.

in Fig. 7. Scavenger receptor-mediated and caveolin-mediated endocytotic pathways are the two processes by which most SNAs enter cells.[29] A549 cells normally take up nanoparticles *via* the caveolin-mediated pathway and the internalized nanoparticles follow the common route: they mature in the late endosomes and are degraded in the lysosomes.[72] Therefore, it is essential to avoid enzymatic degradation in lysosomal compartments. There are evidences that the nanoparticles could bypass lysosomal degradation and vesicles' cargo can be delivered to various cellular destinations (endoplasmic reticulum, Golgi apparatus, *etc.*).[72] However, larger particles (*e.g.*, structures greater than 25 nm in diameter and over 500 kDa in molar mass), even if able to escape the lysosomes, typically do not enter the nucleus. Despite of their relatively large size (see Fig. 5 and Table 2), the DPPC/Chol/NucL2 vesicles have the advantage of their non-covalent architecture and dynamic structure, which could lead to release of intact nucleolipid molecules that could reach and enter the nucleus. Incorporating of hydrophobically modified antisense oligonucleotides into liposomal SNAs have recently been hypothesized and evaluated in the context of antisense regulation of long-noncoding RNAs.[29]

Conclusions

We have designed and synthesized an original nucleolipid, composed of a lipid-mimetic residue covalently attached to a DNA oligonucleotide strand. The novel nucleolipid was synthesized *via* an initiator-free azide–alkyne *click* coupling reaction of appropriately functionalized species – a lipid-mimetic anchor DHP (1,3-dihexadecyloxy-propane-2-ol) and a short (21 bases) single stranded oligonucleotide with non-specific sequence. The functionalization of DHP required introduction of a short spacer of six EO units, because the direct conversion of the secondary hydroxyl group in DHP to mesylate and, then, azide groups was found to be ineffective. Importantly, the strain of the alkyne ring of dibenzocyclooctyne-terminated oligonucleotide was employed to conjugate the latter to the azido-finctionalized DHP thus avoiding copper catalysis. Upon conjugation of species with opposite water solubility, amphiphilic properties of the resulting nucleolipid were conferred. In aqueous solution, the nucleolipid was found to self-associate into supramolecular structures identified as self-closed interdigitated bilayers densely (100%) grafted with oligonucleotide strands and characterized by a relatively large size (R_h = 115.1 nm), molar mass ($M_w = 709.0 \times 10^6$ g mol^{-1}) and aggregation number ($N_{agg} = 8.8 \times 10^4$), and strongly negative (−31.9 mV) ζ potential. Another type of vesicular structures were successfully prepared by co-assembly of the novel nucleolipid with readily available lipids 1,2-dipalmitoyl-*sn-glycero*-phosphocholine and cholesterol. They were obtained by the common route for preparation of small unilamellar liposomes (thin film hydration, freeze-thawing, and multiple extrusion through small pore size filters) and their vesicular structure was revealed by cryo-TEM. The vesicles were found to carry thousands (an average of 3430 ± 92) of oligonucleotide strands per particle anchored in the bilayer membrane at a grafting density that was slightly lower than the grafting density at the transition to the brush regime implying unextended conformation of the strands. The grafting density, however, can be increased and the strands can adopt a more extended conformation upon increasing nucleolipid content in the formulations. The shell of oligonucleotide strands endowed the two vesicular structures with properties similar to those of the spherical nucleic acids. They exhibited enhanced nuclease stability and ability to cross the cell membranes without the need of transfection agents. Considering the resistance of the structures to enzymatic degradation, one may anticipate enhanced stability in biological media at physiological conditions that would increase their lifetime.

Author contributions

Conceptualization, Stanislav Rangelov and Natalia Toncheva-Moncheva; data curation, Erik Dimitrov, Pavel Bakardzhiev, Aleksander Forys, Kirilka Mladenova; formal analysis, Erik Dimitrov, Pavel Bakardzhiev, Aleksander Forys, Kirilka Mladenova, and Jordan Doumanov; funding acquisition, Stanislav Rangelov, Jordan Doumanov, and Natalia Toncheva-Moncheva; investigation, Erik Dimitrov, Natalia Toncheva-Moncheva, Pavel Bakardzhiev, Aleksander Forys, Kirilka Mladenova, Svetla Petrova, Jordan Doumanov, Barbara Trzebicka, and Stanislav Rangelov; methodology, Erik Dimitrov, Aleksander Forys, Svetla Petrova, Kirilka Mladenova, Pavel Bakardzhiev; project administration, Stanislav Rangelov, Natalia Toncheva-Moncheva, and Jordan Doumanov; resources, Stanislav Rangelov and Jordan Doumanov; supervision, Stanislav Rangelov, Barabara Trzebicka, Svetla Petrova, and Jordan Doumanov; validation, Erik Dimitrov, Pavel Bakardzhiev, Aleksander Forys, Kirilka Mladenova and Natalia Toncheva-Moncheva; writing – original draft, Natalia Toncheva-Moncheva and Stanislav Rangelov; writing – review and editing, Erik Dimitrov, Natalia Toncheva-Moncheva, Pavel Bakardzhiev, Aleksander Forys, Jordan Doumanov, Kirilka Mladenova, Svetla Petrova, Barbara Trzebicka, and Stanislav Rangelov.

Conflicts of interest

There are no conflicts to declare.

Acknowledgements

This work was supported by the National Science Fund (Bulgaria) project no DN19/8-2017. Research equipment of Distributed Research Infrastructure INFRAMAT, part of the Bulgarian National Roadmap for Research Infrastructures, supported by the Bulgarian Ministry of Education and Science, was used in this investigation.

References

1 C. A. Mirkin, R. L. Letsinger, R. C. Mucic and J. J. Storhoff, *Nature*, 1996, **382**, 607.

2 J. I. Cutler, E. Auyeung and C. A. Mirkin, *J. Am. Chem. Soc.*, 2012, **134**, 1376.
3 C. H. Chung, J. H. Kim, J. Jung and B. H. Chung, *Biosens. Bioelectron.*, 2013, **41**, 827.
4 C. H. Choi, L. Hao, S. P. Narayan, E. Auyeung and C. A. Mirkin, *Proc. Natl. Acad. Sci. U. S. A.*, 2013, **110**, 7625.
5 M. D. Massich, D. A. Giljohann, A. L. Schmucker, P. C. Patel and C. A. Mirkin, *ACS Nano*, 2010, **4**, 5641.
6 C. Guan, N. Chernyak, D. Dominguez, L. Cole, B. Zhang and C. A. Mirkin, *Small*, 2018, **14**, e1803284.
7 W. Ruan, M. Zheng, Y. An, Y. Liu, D. B. Lovejoy, M. Hao, Y. Zou, A. Lee, S. Yang, Y. Lu, M. Morsch, R. Chung and B. Shi, *Chem. Commun.*, 2018, **54**, 3609.
8 R. J. Banga, B. Meckes, S. P. Narayan, A. J. Sprangers, S. T. Nguyen and C. A. Mirkin, *J. Am. Chem. Soc.*, 2017, **139**, 4278.
9 J. R. Melamed, N. L. Kreuzberger, R. Goyal and E. S. Day, *Mol. Ther.–Nucleic Acids*, 2018, **12**, 207–219.
10 S. A. Jensen, E. S. Day, C. H. Ko, L. A. Hurley, J. P. Luciano, F. M. Kouri, T. J. Merkel, A. J. Luthi, P. C. Patel, J. I. Cutler, W. L. Daniel, A. W. Scott, M. W. Rotz, T. J. Meade, D. A. Giljohann, C. A. Mirkin and A. H. Stegh, *Sci. Transl. Med.*, 2013, **5**, 1.
11 C. A. Mirkin and S. H. Petrosko, *Clin. Chem.*, 2018, **64**, 971–972.
12 G. Yamankurt, E. J. Berns, A. Xue, A. Lee, N. Bagheri, M. Mrksich and C. A. Mirkin, *Nat. Biomed. Eng.*, 2019, **3**, 318.
13 D. Bousmail, L. Amrein, J. J. Fakhoury, H. H. Fakih, J. C. C. Hsu, L. Panasci and H. F. Sleiman, *Chem. Sci.*, 2017, **8**, 6218.
14 L. Hao, P. C. Patel, A. H. Alhasan, D. A. Giljohann and C. A. Mirkin, *Small*, 2011, **7**, 3158.
15 J. S. Lee, A. K. R. Lytton-Jean, S. J. Hurst and C. A. Mirkin, *Nano Lett.*, 2007, **7**, 2112.
16 J. L. Cutler, D. Zheng, X. Y. Xu, D. A. Giljohann and C. A. Mirkin, *Nano Lett.*, 2010, **10**, 1477.
17 G. P. Mitchell, C. A. Mirkin and R. L. Letsinger, *J. Am. Chem. Soc.*, 1999, **121**, 8122.
18 C. Zhang, R. J. Macfarlane, K. L. Young, C. H. J. Choi, L. Hao, E. Auyeung, G. Liu, X. Zhou and C. A. Mirkin, *Nat. Mater.*, 2013, **12**, 741.
19 K. L. Young, A. W. Scott, L. Hao, S. E. Mirkin, G. Liu and C. A. Mirkin, *Nano Lett.*, 2012, **12**, 3867.
20 C. Xue, X. Chen, S. J. Hurst and C. A. Mirkin, *Adv. Mater.*, 2007, **19**, 4071.
21 C. H. Rische, A. Goel, A. F. Radovic-Moreno and S. M. Gryaznov, *Mater. Today Commun.*, 2016, **9**, 30.
22 D. Yao, T. Song, X. Sun, S. Xiao, F. Huang and H. Liang, *J. Am. Chem. Soc.*, 2015, **137**, 14107.
23 R. J. Banga, N. Chernyak, S. P. Narayan, S. T. Nguyen and C. A. Mirkin, *J. Am. Chem. Soc.*, 2014, **136**, 9866.
24 J. D. Brodin, E. Auyeung and C. A. Mirkin, *Proc. Natl. Acad. Sci. U. S. A.*, 2015, **112**, 4564.
25 K. J. Watson, S. J. Park, J. H. Im, S. T. Nguyen and C. A. Mirkin, *J. Am. Chem. Soc.*, 2001, **123**, 5592.
26 Z. Li, Y. Zhang, P. Fullhart and C. A. Mirkin, *Nano Lett.*, 2004, **4**, 1055.
27 X. Tan, X. Lu, F. Jia, X. Liu, Y. Sun, J. K. Logan and K. Zhang, *J. Am. Chem. Soc.*, 2016, **138**, 10834.
28 R. J. Banga, S. A. Krovi, S. P. Narayan, A. J. Sprangers, G. Liu, C. A. Mirkin and S. T. Nguyen, *Biomacromolecules*, 2017, **18**, 483.
29 A. J. Sprangers, L. Hao, R. J. Banga and C. A. Mirkin, *Small*, 2017, **13**, 1602753.
30 H. Rosemeyer, *Chem. Biodiversity*, 2005, **2**, 977.
31 L. Simeone, G. Mangiapia, C. Irace, A. Di Pascale, A. Colonna, O. Ortona, L. De Napoli, D. Montesarchio and L. Paduano, *Mol. BioSyst.*, 2011, **7**, 3075.
32 A. Gissot, M. Camplo, W. G. Mark and P. Barthelemy, *Org. Biomol. Chem.*, 2008, **6**, 1324.
33 S. Milani, D. Berti, S. Dante, T. Hauss and P. Baglioni, *Langmuir*, 2009, **25**, 4084.
34 N. Taib, A. Aimé, S. Houmadi, S. Castano, Ph. Barthélémy, M. Laguerre and I. Bestel, *Langmuir*, 2012, **28**, 7452.
35 E. Lepeltier, C. Bourgaux, V. Rosilio, J. H. Poupaert, F. Meneau, F. Zouhiri, S. Lepetre-Mouelhi, D. Desmaele and P. Couvreur, *Langmuir*, 2013, **29**, 14795.
36 V. Allain, C. Bourgaux and P. Couvreur, *Nucleic Acids Res.*, 2012, **40**, 1891.
37 C. Gosse, A. Boutorine, I. Aujard, M. Chami, A. Kononov, E. Cogné-Laage, J.-F. Allemand, J. Li and L. Jullien, *J. Phys. Chem. B*, 2004, **108**, 6485.
38 J. S. Nowick, J. S. Chen and G. Noronha, *J. Am. Chem. Soc.*, 1993, **115**, 7636.
39 J. S. Nowick, T. Cao and G. Noronha, *J. Am. Chem. Soc.*, 1994, **116**, 3285.
40 R. G. Shea, J. C. Marsters and N. Bischofberger, *Nucleic Acids Res.*, 1990, **18**, 3777.
41 E. T. Rump, R. L. A. de Vrueh, L. A. J. M. Sliedregt, E. A. L. Biessen, T. J. C. van Berkel and M. K. Bijsterbosch, *Bioconjugate Chem.*, 1998, **9**, 341.
42 S. Rangelov, E. Petrova, I. Berlinova and C. Tsvetanov, *Polymer*, 2001, **42**, 4483.
43 P. Bakardzhiev, S. Rangelov, B. Trzebicka, D. Momekova and G. Lalev, *RSC Adv.*, 2014, **4**, 37208.
44 S. W. Provencher, *Macromol. Chem.*, 1979, **180**, 201.
45 Q. He, J. Liu, X. Sun and Z. R. Zhang, *World J. Gastroenterol.*, 2004, **10**, 660.
46 H. Li, B. Zhang, X. Lu, X. Tan, F. Jia, Y. Xiao, Z. Cheng, Y. Li, D. O. Silva, H. S. Schrekker, K. Zhang and C. A. Mirkin, *Proc. Natl. Acad. Sci. U. S. A.*, 2018, **115**, 4340.
47 T. Enoki, V. M. Henriques and T. V. M. Lamy, *Chem. Phys. Lipids*, 2012, **165**, 826.
48 L. N. d. M. Ribeiro, V. M. Couto, L. F. Fraceto and d. E. Paula, *Sci. Rep.*, 2018, **8**, 982.
49 W. Burchard, *Adv. Polym. Sci.*, 1983, **48**, 1.
50 A. Thurn, W. Burchard and R. Niki, *Colloid Polym. Sci.*, 1987, **265**, 653.
51 K. Hristova and D. Needham, *Macromolecules*, 1995, **28**, 991.
52 J. Y. Huang and G. W. Feigenson, *Biophys. J.*, 1999, **76**, 2142.
53 J. A. Clarke, A. J. Heron, J. M. Seddon and R. V. Law, *Biophys. J.*, 2006, **90**, 2383.
54 P. Bakardzhiev, A. Forys, B. Trzebicka, T. Andreeva and S. Rangelov, *Nanoscale*, 2021, **13**, 15210.

55 D. D. Lasic, *Biochem. J.*, 1988, **256**, 1.
56 Y. P. Patil and S. Jadhav, *Chem. Phys. Lipids*, 2014, **177**, 8.
57 Y. Barenholz, *Curr. Opin. Colloid Interface Sci.*, 2001, **6**, 66.
58 W. M. Li, L. Xue, L. D. Mayer and M. B. Bally, *Biochim. Biophys. Acta*, 2001, **1513**, 193.
59 A. Kenworthy, K. Hristova, D. Needham and T. J. McIntosh, *Biophys. J.*, 1995, **68**, 1921.
60 J. F. Nagle and S. Tristram-Nagle, *Biochim. Biophys. Acta*, 2000, **1469**, 159.
61 A. Magarkar, V. Dhawan, P. Kallinteri, T. Viitala, M. Elmowafy, T. Róg and A. Bunker, *Sci. Rep.*, 2014, **4**, 5005.
62 P. Bakardzhiev, D. Momekova, K. Edwards, S. Konstantinov and S. Rangelov, *J. Drug Delivery Sci. Technol.*, 2015, **29**, 90.
63 T. A. Taton, C. A. Mirkin and R. L. Letsinger, *Science*, 2000, **289**, 1757.
64 C. M. Calabrese, T. J. Merkel, W. E. Briley, P. S. Randeria, S. P. Narayan, J. L. Rouge, D. A. Walker, A. W. Scott and C. A. Mirkin, *Angew. Chem., Int. Ed.*, 2015, **54**, 476.
65 S. J. Hurst, A. K. R. Lytton-Jean and C. A. Mirkin, *Anal. Chem.*, 2006, **78**, 8313.
66 E. Haladjova, I. Ugrinova and S. Rangelov, *Soft Matter*, 2020, **16**, 191.
67 N. L. Rosi, D. A. Giljohann, C. S. Thaxton, A. K. Lytton-Jean, M. S. Han and C. A. Mirkin, *Science*, 2006, **312**, 1027.
68 W. Briley, T. L. Halo, P. S. Randeria, A. H. Alhasan, E. Auyeung, S. J. Hurst, and C. A. Mirkin, in Nanomaterials for Biomedicine, ACS Symposium Series, ed. R. Nagarajan, American Chemical Society, Washington, DC, 2012, pp. 1–20.
69 X. A. Wu, C. H. J. Choi, C. Zhang, L. Hao and C. A. Mirkin, *J. Am. Chem. Soc.*, 2014, **136**, 7726.
70 F. Sakurai, T. Nishioka, H. Saito, T. Baba, A. Okuda, O. Matsumoto, T. Taga, F. Yamashita, Y. Takakura and M. Hashida, *Gene Ther.*, 2001, **8**, 677.
71 C. Poojari, N. Wilkosz, R. B. Lira, R. Dimova, P. Jurkiewicz, R. Petka, M. Kepczynski and T. Róg, *Chem. Phys. Lipids*, 2019, **223**, 104784.
72 Sh. Behzadi, V. Serpooshan, W. Tao, M. A. Hamaly, M. Y. Alkawareek, E. C. Dreadene, D. Brown, A. M. Alkilany, O. C. Farokhzad and M. Mahmoudi, *Chem. Soc. Rev.*, 2017, **46**, 4218.